Chapter 6 *Structure and Resistive Switching Behavior of Molecular Beam Epitaxy Grown HfO_2 Thin Films*

6.1 Introduction

In this chapter, we have observed the structure, morphology and resistive switching behavior of molecular beam epitaxy (MBE) grown HfO_2 thin films fabricated on p^{++}-Si (100) substrate at substrate temperature of 300 and 500 °C. The detailed insights into the structure and microstructure of these films are provided in section 6.2. Volatile resistive switching behavior of these MBE grown HfO_2 films are discussed in section 6.3. Both films demonstrate forming free volatile resistive switching behavior with SET voltage of -3.1 and -3.6 V, along with the ON/OFF ratio of ~ 2 and ~ 4 for the films with substrate temperature of 300 and 500 °C, respectively. Memory device based on HfO_2 film with higher substrate temperature exhibits a better ON/OFF ratio due to higher crystallinity and availability of more oxygen vacancies. A comprehensive mechanism of resistive switching is also discussed in this chapter, considering the transport of Ag ions and oxygen vacancies. In section 6.4, we have summarized the key findings of this chapter.

6.2 Structure and Microstructure

6.2.1 Structure through Grazing Incidence X-ray Diffraction

Molecular beam epitaxy grown HfO_2 films, fabricated on p^{++}-Si (100) at substrate temperatures of 300 and 500 °C, ascribed as Film A and Film B, respectively. **Figure 6.1** depicts the grazing incidence X-ray diffraction (GIXRD) patterns of the HfO_2 thin films, recorded at a grazing angle = 0.5°.

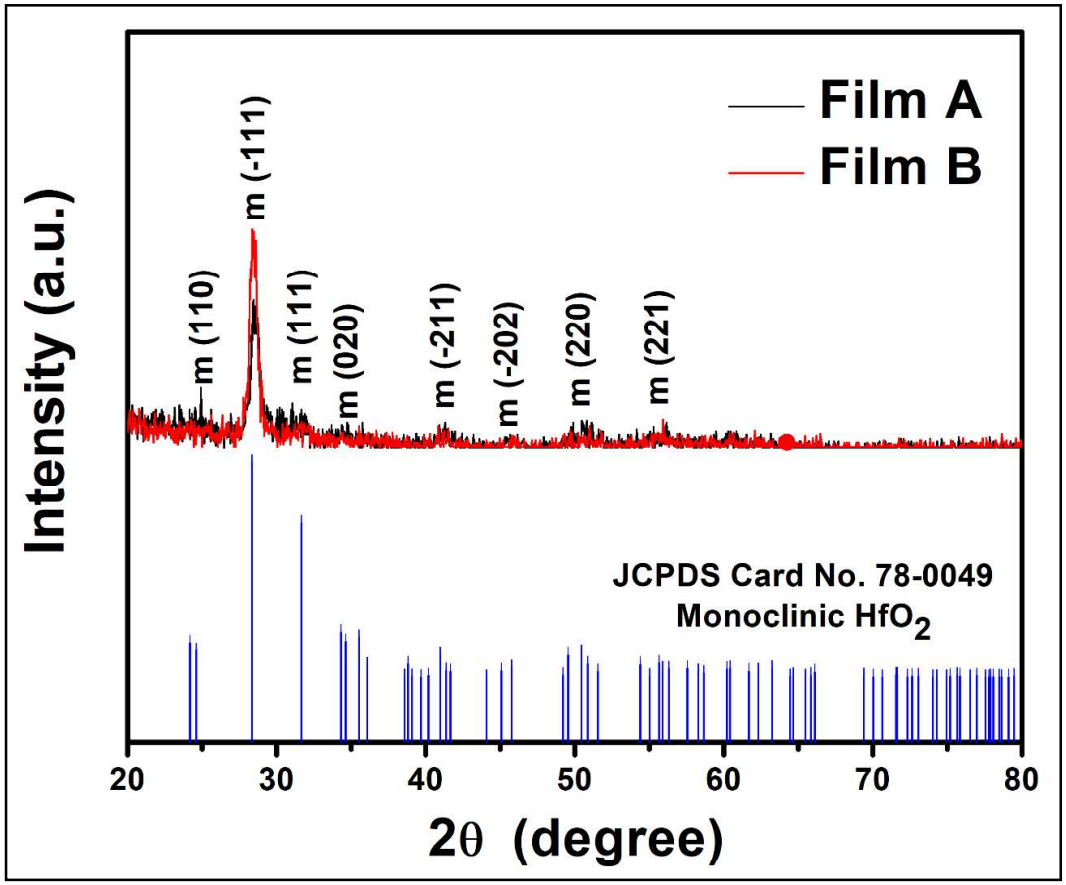

Figure 6.1 *GIXRD patterns for HfO_2 thin films deposited at substrate temperature of 300 (Film A) and 500 °C (Film B) along with the standard JCPDS data.*

The GIXRD patterns of both Film A and Film B exhibit diffraction peaks at 24.8°, 28.4°, 31.6°, 34.5°, 41.1°, 45.8°, 50.6° and 55.6°, corresponding to (110), (-111), (111), (020), (-211), (-202), (220) and (221), respectively, representing the monoclinic phase (m-phase) of HfO_2 with space group $P2_1/c$ (JCPDS card no. 78-0049). There are no extra peaks present in the GIXRD patterns, which confirms the pure monoclinic phase. In addition, both the films have preferred growth orientation along (-111), showing the single crystalline behavior. With the increase in the substrate temperature, the crystallinity of the film increases, as can be seen from the intensity of the GIXRD patterns. The surface temperature is the most important parameter during the molecular

beam epitaxy growth process since it influences the surface morphology, the crystallinity, the incorporation kinetics and the redistribution of the dopants.

6.2.2 Thickness, Density and Roughness by X-ray Reflectivity

X-ray reflectometry (XRR) spectra for Film A and Film B are shown in **Figure 6.2 (a)** and **(b)**. We have fitted the experimental XRR data using appropriate stack models with Parratt32 software. The fittings demonstrate that in both the films, the observed XRR spectra and simulated data are in good agreement with each other. An interfacial layer of hafnium silicate having thickness 3 and 2 nm is observed in the case of Film A and Film B, respectively. The calculated thickness of HfO_2 layer is found to be 31 and 33 nm, whereas the density is determined to be 9.1 and 9.2 g/cm^3 corresponding to Film A and

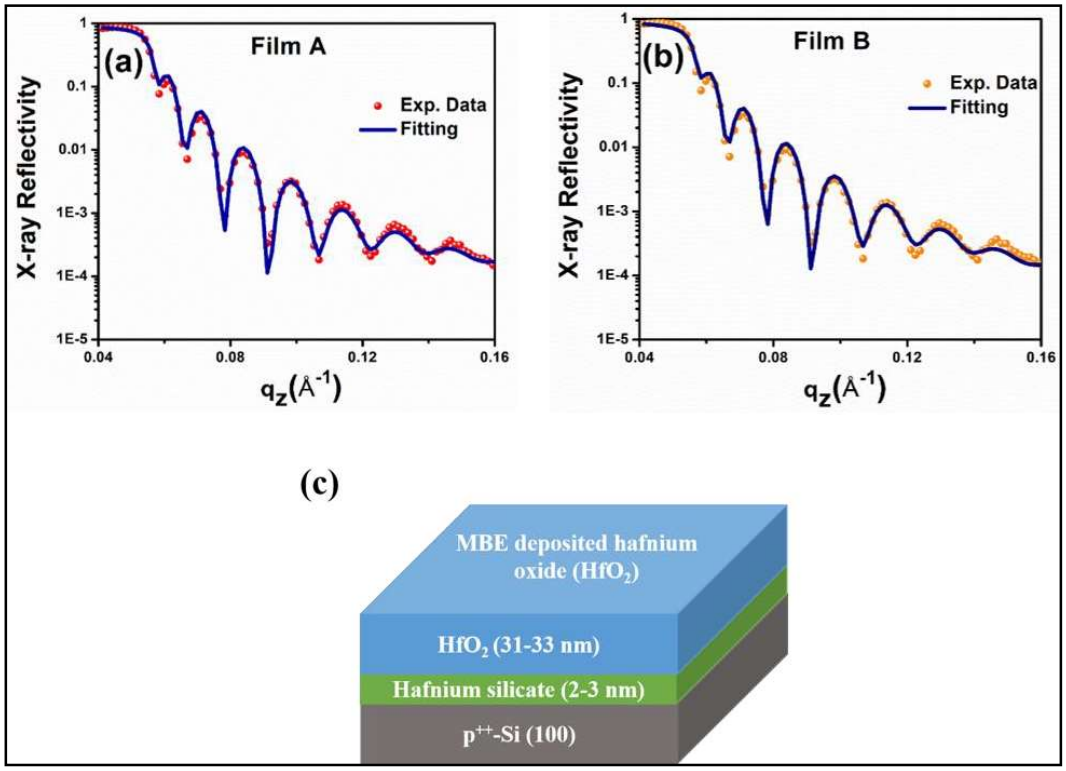

Figure 6.2 *(a,b) X-ray reflectivity spectra for film A and Film B and (c) schematic diagram of the stacking model.*

Film B, respectively. The surface roughness is estimated to be 1.41 nm for Film A, whereas it is 2.36 nm for Film B. The schematic diagram of stacking model obtained from the XRR fitting is shown in **Figure 6.2 (c)**.

6.2.3 Surface Morphology by Atomic Force Microscopy

The topography of the HfO_2 layer extremely important since a smooth surface with dense grains and less porosity makes the HfO_2 film more efficient in the memory cell. Atomic force microscopy (AFM) is used to obtain the surface morphology of the thin films. The 2D and 3D AFM images of Film A and Film B are depicted in **Figure 6.3**.

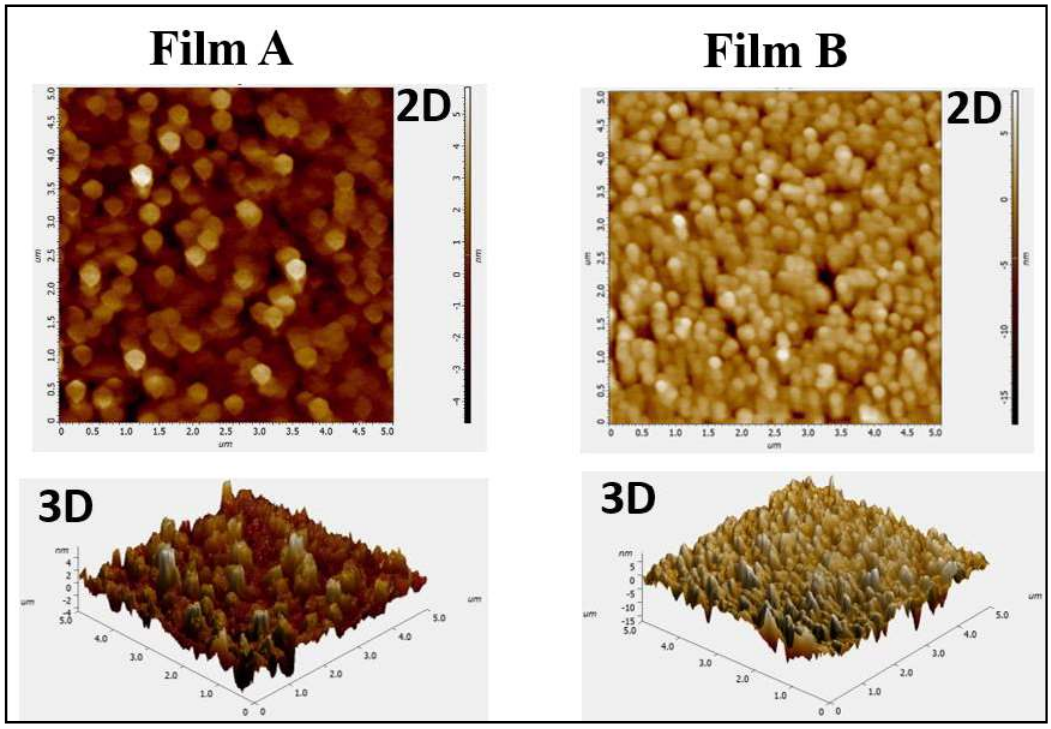

Figure 6.3 *2D and 3D AFM micrographs of the Film A and Film B.*

The average grain size of both the films is found to be ~ 140 nm. The root mean square roughness of Film A and Film B is found to be 1.34 and 2.4 nm, respectively, which are

very close to the roughness estimated from the XRR spectra. The minimum surface roughness plays a substantial role in minimizing the leakage current in the electronic devices and supports the local charge transport [150].

6.2.4 Auger Electron and X-ray Photoelectron Spectroscopy

To study the oxidation states of hafnium and oxygen vacancy concentration of the HfO_2 thin films, in-situ Auger electron spectroscopy (AES) is employed. AES data for Film A and Film B is depicted in **Figure 6.4**. The kinetic energy (KE) of Hf_{NOO} and O_{KLL} transitions are observed at ~ 100 and 510 eV, respectively, in the AES spectra [167,168]. Here, there is no peak observed at ~ 100 eV and a very less intense peak exists at ~ 510 eV. Therefore, we have carried out X-ray photoelectron spectroscopy (XPS).

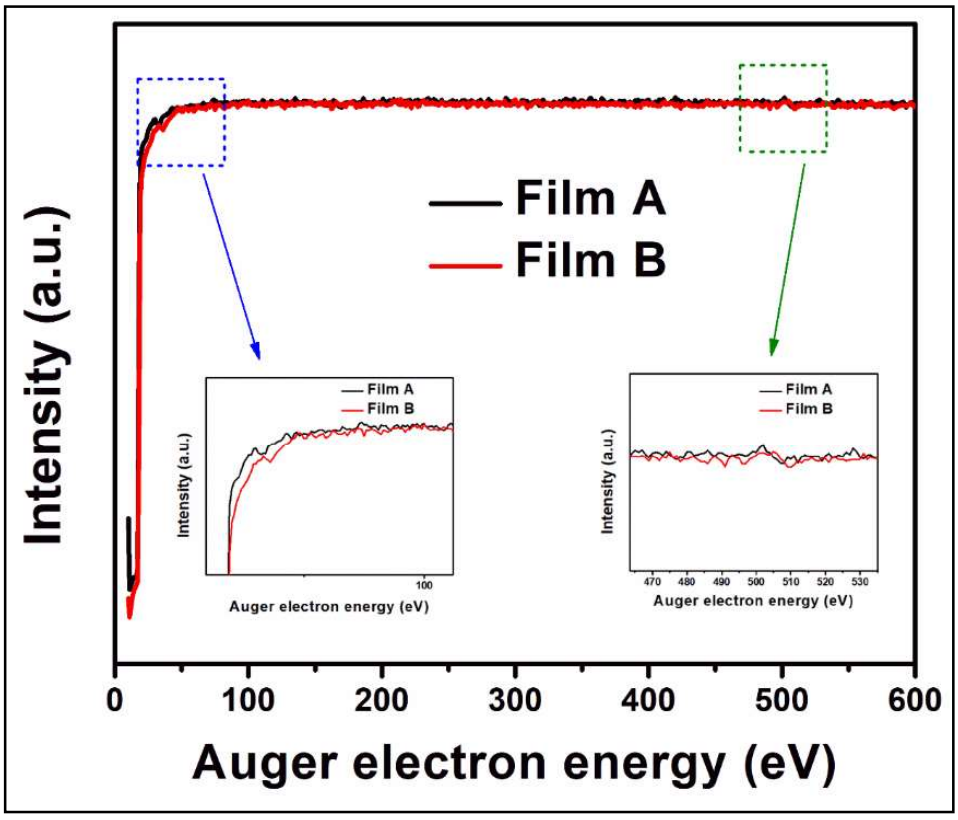

Figure 6.4 *Auger electron spectra of the HfO_2 films.*

Prior to the analysis, all the XPS spectra are corrected with respect to the C 1*s* peak located at ~ 284.6 eV. **Figure 6.5 (a)** and **(b)** show the XPS spectra of Hf 4*f* core levels for Film A and Film B, which are deconvoluted into two peaks having mixed Gaussian and Lorentzian functions. The two peaks are found to be located at ~ 16.3 and ~ 18 eV associated to Hf $4f_{7/2}$ and Hf $4f_{5/2}$, respectively [105]. The separation of 1.68 eV between Hf $4f_{7/2}$ and Hf $4f_{5/2}$ indicates the presence of 4+ valence state of Hf [169].

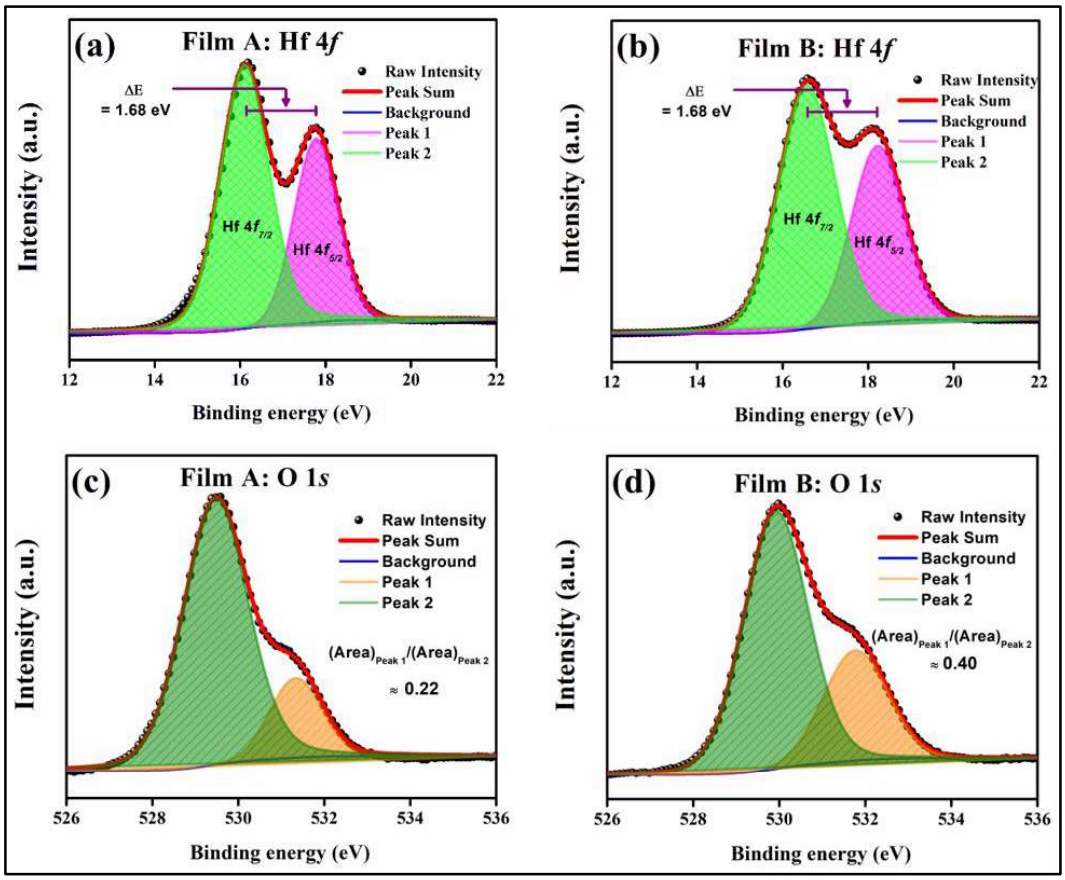

Figure 6.5 *(a,b) Hf 4f and (c,d) O 1s core level XPS spectra of Film A and Film B.*

XPS spectra of O 1*s* for Film A and Film B are demonstrated in **Figure 6.5 (c)** and **(d)**. Due to asymmetric shape of the O 1*s* spectra, we have deconvoluted the spectra into two peaks named as Peak 1 and Peak 2, centered at ~ 531.5 and ~ 529.7 eV, respectively. In

the higher binding energy (BE) region, the peak at ~ 531.5 eV is attributed to oxygen deficient regions exhibiting oxygen vacancies and oxygen in Si-O bonds, whereas the lower BE peak at ~ 529.7 is ascribed to lattice oxygen atoms in Hf-O bonds [29,147,153]. The ratio of area under Peak 1 and Peak 2, i.e., $[(\text{Area})_{\text{Peak 1}}/(\text{Area})_{\text{Peak 2}}]$, is found to be 0.22 and 0.40 for Film A and Film B, respectively. The oxygen vacancy concentration is higher in Film B than that of Film A, which can be accredited to the higher growth temperature under vacuum in Film B.

6.3 Resistive Switching Behavior

6.3.1 Current-Voltage (*I-V*) Characteristics

The role of the structure, morphology and electromigration of oxygen vacancies/metal ions have been examined for the performance of HfO_2 thin film based memristors. We have measured *I-V* cycles to study the resistive switching (RS) behavior of the HfO_2 films using Ag as the top electrode material. After sweeping the applied DC bias voltage in a cycle of 0 V → -4 V → 0 V → 1 V → 0 V, *I–V* measurements are carried out. The bias voltage is applied to the top electrode while the bottom electrode is grounded throughout the measurement. The compliance current during switching measurement has been set at 100 μA to prevent the electrical breakdown of the device. The schematic diagram of the memristor device for *I-V* measurements is shown in **Figure 6.6 (a)**. The device-to-device variation plots do not show significant variation among the five devices of the same film (**Figure 6.6 (b)**). **Figure 6.6 (c)** shows the 1st, 50th and 100th *I-V* cycles for Film A. The SET voltage is found to be -3.1 V with an ON/OFF ratio of ~ 2 for Film A. Similarly, the schematic diagram, device-to-device variation and *I-V* characteristics for Film B is represented in **Figure 6.7 (a)** to **(c)**.

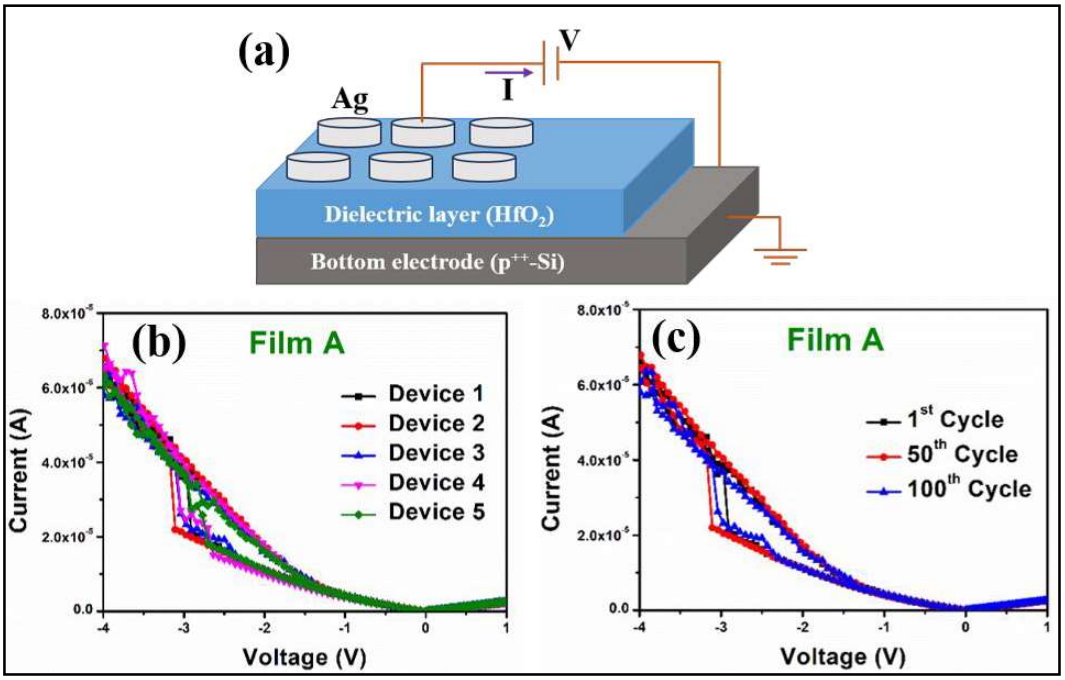

Figure 6.6 *(a) Schematic diagram, (b) device-to-device variation and (c) 1st, 50th and 100th I-V cycles of the memristor based on Film A.*

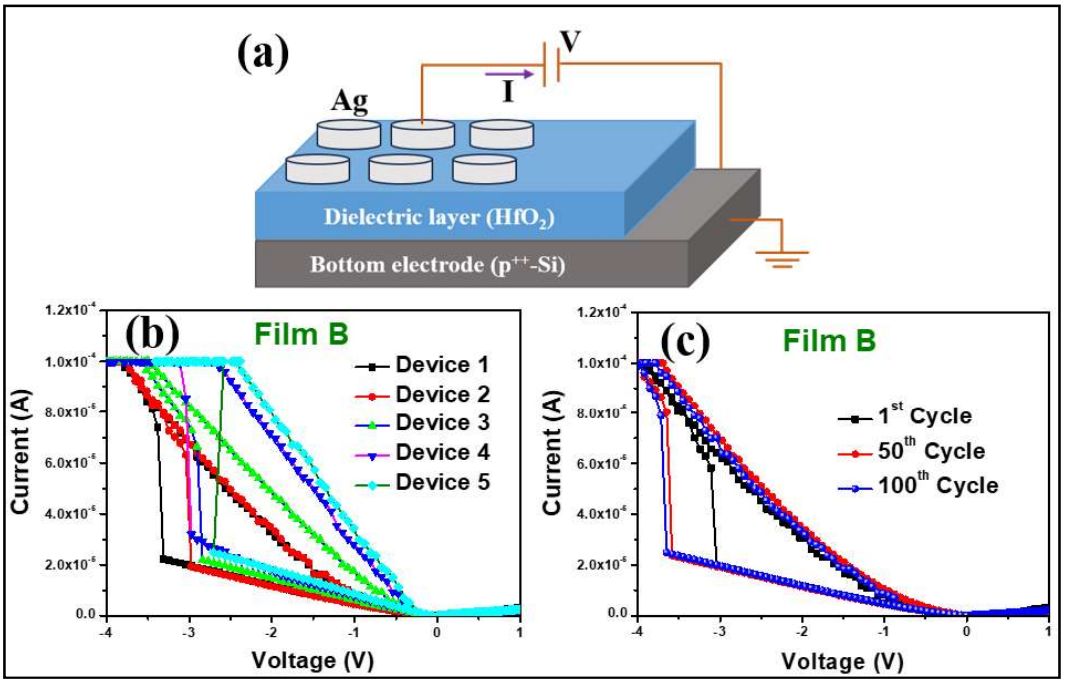

Figure 6.7 *(a) Schematic diagram, (b) device-to-device variation and (c) 1st, 50th and 100th I-V cycles of the memristor based on Film B.*

The SET voltage is estimated as -3.6 V and separation between ON and OFF states as ~ 4 for Film B. From the *I-V* plots, we can confirm that the memristors based on both Film A and Film B are volatile in nature. The *I-V* cycle from 0 V → -5 V → 0 V → 5 V → 0 V for Film B is shown in **Figure 6.8**, which shows the resistive switching only on the negative bias volage confirming the volatile behavior.

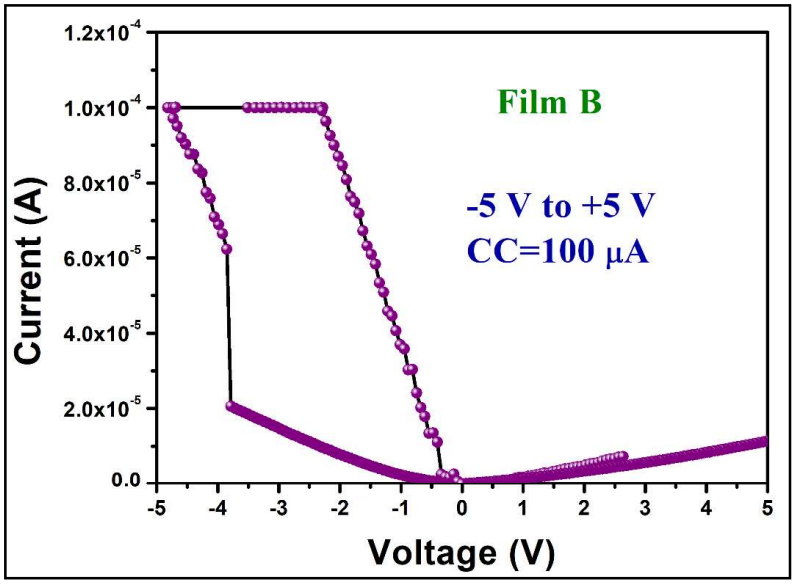

Figure 6.8 *I-V characteristics for Film B in the applied voltage range of 0 V → -5 V → 0 V → 5 V → 0 V.*

6.3.2 Mechanism for Restive Switching

The formation of conductive filaments (CFs) through migration of oxygen vacancies/oxygen ions, Schottky barrier, and trapped charged carriers has mostly been used to explain the resistive switching behavior [163]. Among them, lots of research is being done on the localized creation and destruction of CFs inside the dielectric active layer. It is well established that localized nanosized CFs are formed in oxide films at low bias voltages, which agglomerate to form stronger and more conductive CFs at higher

applied bias voltages. Zhang *et al.* explore that RRAM behavior increases through Gd doping in the HfO_2 lattice by diminishing the randomized characteristic of CFs, thus minimizing the barrier of oxygen ion migration [164]. The report by Lee *et al.* reveals that Gd and Dy doped ZrO_2 devices display switching behavior because of the adequately large concentration of oxygen vacancies induced by the dopants, while Ce doped ZrO_2 based RRAM demonstrates the preliminary formation of CF, which is attributed to enhanced crystallization [160]. To verify the experimental evidence, a theoretical model has been proposed by Rozenberg *et al.* that accounts for the bipolar resistive switching phenomenon observed in transition metal oxides [165]. This model assumes three key features: (a) electric transport dominated by a single conductive path embedded within a more insulating host, (b) relevance of the significant number of oxygen vacancy (V_o) defects within the dielectric, and (c) role of interface between the dielectric and the metallic electrode, to correctly reproduce the hysteresis cycles. It qualitatively describes the electric field enhanced migration of oxygen vacancies at the nanoscale. The presence of an appropriately high concentration of V_os, along with enhanced crystallization in Film B, predominantly contributes to better resistive switching behavior. The **Figure 6.9** shows a schematic illustration of RS mechanism for the volatile memory devices by the formation of conducting filaments consisting of oxygen vacancies and electromigration of Ag ions. At zero bias voltage, the memory device is at the HRS state where V_os are randomly oriented in the HfO_2 film. These positively charged V_os move towards the top electrode (TE) and accumulate there when a negative bias is applied to the TE. The accumulating V_os transform into the nuclei of CFs since V_os may produce an acceptor level close to the valence band, which is the origin of hole-electron carriers. These nuclei subsequently expand towards the bottom electrode (BE) and act as extensions of the TE. The memory device switches into the LRS state once a complete CF has formed. When

the TE is positively biased, the majority of the Joule heat is produced at the TE end of the CF, thereby substantially fast-tracking the mobility of V_os in this area. V_os in this area move fast towards the BE under the influence of the electric field and are annihilated by the oxygen ions present at the active layer/BE interface or at the grain boundaries of the BE. Consequently, the concentration of V_os in the TE end of the CF is reduced considerably, leading to the rupture (destruction) of the CF at that site, resulting in the switching of the memory cell to the HRS state. Thus, it is concluded that volatile memristor based on Film B shows well-regulated resistive switching behavior due to the enhanced crystallization and abundance of oxygen vacancies. The conduction mechanism is same for the conductive filaments consisting of Ag ions. Here, while sweeping back from -4 V to 0 V, the device transits from LRS to HRS resulting in volatile resistive switching. In other words, the LRS is not maintained after removing the applied electric field. These volatile switching devices can be utilized for next-generation data storage as well as in neuromorphic computing devices to emulate several synaptic functions.

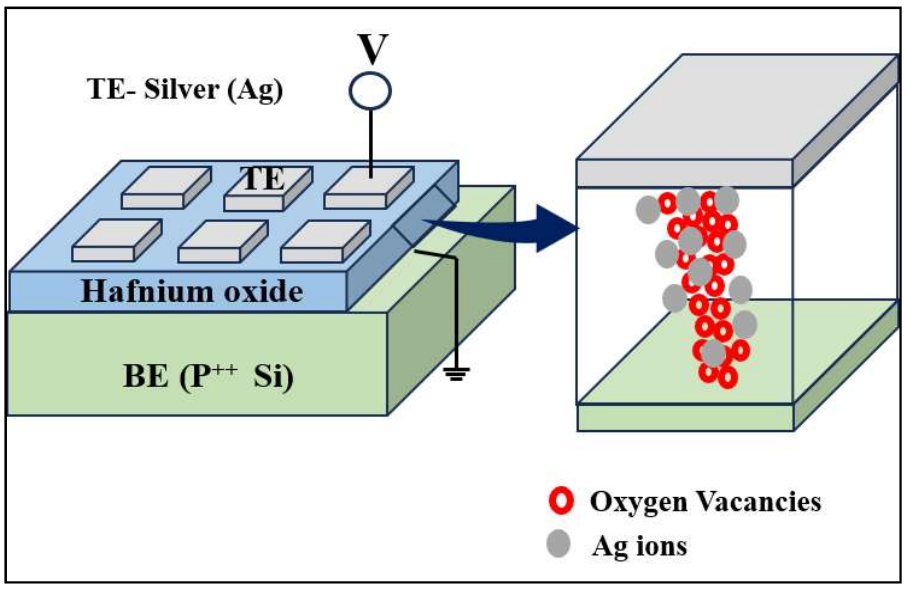

Figure 6.9 *Resistive switching mechanism for volatile memristor.*

6.4 Conclusions

In conclusion, we investigated the structure, morphology and resistive switching behavior of molecular beam epitaxy grown HfO_2 thin films fabricated on p^{++}-Si (100) substrate at substrate temperature of 300 and 500 °C. The crystalline nature and monoclinic phase ($P2_1/c$) of the HfO_2 films were confirmed by the GIXRD patterns. The density of the HfO_2 layer was found to be 9.1 and 9.2 g/cm^3 in the films with substrate temperature of 300 and 500 °C, respectively, along with an interfacial hafnium silicate layer. The root mean square roughness of HfO_2 films deposited at substrate temperature of 300 and 500 °C were found to be 1.34 and 2.40 nm with average grain size of 140 nm in both films. To obtain detailed insights into the resistive switching behavior, 100 *I-V* cycles were recorded with Ag as the top electrode. Both films demonstrated forming free volatile resistive switching behavior with SET voltage of -3.1 and -3.6 V, whereas the ON/OFF ratio was found to be ~ 2 and ~ 4 for the films with substrate temperature of 300 and 500 °C, respectively. Memory device based on HfO_2 film with higher substrate temperature exhibited a better ON/OFF ratio due to the higher crystallinity and availability of more oxygen vacancies. A comprehensive mechanism of resistive switching was also discussed in this chapter.